

## ANALYSIS OF TRANSPORT BARGE NONLINEAR ROLL MOTIONS IN A SEAWAY USING AN EQUIVALENT LINEARIZATION PROCEDURE

**Allen H. Magnuson**

Principal Naval Architect and Offshore Engineer  
Bastion Technologies  
Houston, Texas 77058, U.S.A.

### ABSTRACT

An investigation of nonlinear barge roll motion using an equivalent linearization procedure was conducted. Barge roll motion data obtained from model tank tests was used for comparison with computed roll response amplitude operators (RAOS). The tests were conducted in regular beam sea waves. A frequency domain roll motion model was implemented for comparison with the model test data. A 3-term time-domain nonlinear roll damping model was converted into a linearized form in the frequency domain using the “equal energy” equivalent linearization procedure. Computed RAOs were compared with the tank test RAOs. After roll peak matching, the comparison showed the computed RAOs consistently showed a narrower resonance peak or “hump”. The 3-term nonlinear damping model proved inadequate to provide the filtering needed to match the computed response with the tank data. Consequently, a suitably designed parabola-shaped mechanical filter was implemented to alter the damping curve to widen the “hump”. It was shown that filter did in fact widen the hump, improving the correlation with test data over the limited frequency range for which the filter was designed. It is suggested that a higher-order time domain damping model, with a corresponding extended equivalent linearization series be developed to improve correlation. A 6<sup>th</sup> or 8<sup>th</sup> order series was felt to be adequate to form a filter with a bell curve shape that would avoid negative damping. Such an extension would improve the correlation to the extent that the linearization technique could be used in spectral work, where the computed RAO area under the spectral integral must match the test tank data. Implementation of this extension would provide a simple, accurate and useful nonlinear roll motion analysis tool.

### 1. INTRODUCTION

It is well known that roll motion of barge-type hull forms under tow in ocean transit can be problematic in heavy seaways. This is especially true for barges heavily loaded with deck cargo, with their high VCG, shallow draft and low freeboard. The current study was conducted because roll motions are still a problem for ocean transport barges. Existing roll motions programs tend to under-predict roll

damping and subsequently, over-predict roll motions. Transport barges are used extensively by industry to transport offshore floating or fixed windmills, drilling rigs, fixed or floating production platforms, and large land-based industrial equipment and facilities. Unlike the other modes of ship motion, the roll motions, especially in barges, are highly nonlinear because of weak roll damping. The roll instability can result in large roll motions in heavy seas which, in turn produce high lateral loads on the deck cargo, the sea fastenings and the barge itself. There is a need for a simple but accurate barge roll motions prediction tool that can model the large amplitude nonlinear behavior, and that can be readily used by shippers. Shippers need these tools to determine in advance the maximum motions and accelerations (particularly in roll) for each voyage. This requires statistical analysis of wind and wave conditions along the proposed route, and an accurate barge motion prediction tool, and spectral analysis.

#### 1.1 Related work

Ibrahim and Grace [1] and El-Bassiouni [2] recently published surveys on ship roll damping. Dhavalikar and Negi [3] recently presented a brief survey on barge roll damping and described ISR’s procedure for estimating barge roll damping. Faltinsen [4], in his useful text on ship sea loads, briefly described and assigned homework problems on the “equal energy” equivalent linearization procedure. Magnuson [5] reanalyzed Japanese barge roll motion data and calculated roll RAOs using data presented in Ando [6]. Ando’s research was translated into English by Latorre [7].

#### 1.2 Current investigation

The author felt that analyzing barge motion characteristics including damping from a phenomenological approach using equivalent linearization should provide valuable insight into nonlinear barge roll motion. As a result, Bastion Technologies recently undertook this investigation as part of an effort to develop new capabilities in the offshore engineering and naval architectural areas. The goal is to develop accurate prediction tools essential for safe barge transport operations.

### 1.3 Nonlinear roll behavior in barges

The nonlinear roll behavior of barges is illustrated in the plot below (Fig. 1) taken from [7]. The peak roll angle is plotted against wave height for seven barge configurations. It can be seen that the peak roll angles tend to level off with increasing wave height. It appears that the marked falloff in roll angle may be caused by the ship literally breaking down the incoming wave. This is a clear indication of very strong nonlinear behavior that is the subject of interest in the current investigation.

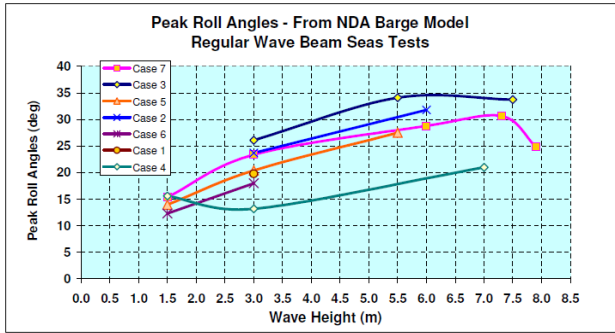


Figure 1 – Peak Roll Angles from NDA Barge Model

### 1.4 Noble Denton & Associates barge motion JIP

In the 1980s, Noble Denton & Associates (Now Noble Denton Group Limited) organized a Joint Industry Project [8] intended primarily to acquire barge motions data and to conduct verification studies on recently-developed ship motions computer programs. At that time, these programs had not been verified to any great extent using ship model wave test data and/or full-scale trials data. Motions programs from eleven different organizations were evaluated, and twenty-five companies sponsored the work. The NDA JIP group organized an extensive program of model-scale tests and data analysis on a systematic series of rectangular barge models. Of particular interest was roll motion data taken well into the nonlinear range. The regular wave roll motion model test data was used to analyze nonlinear roll damping using, among other things, equivalent linearization

### 1.4 Description of the NDA JIP barge series

A standard barge configuration representing a typical oceangoing barge was designed as the parent for the series. A sketch of the standard barge, courtesy NDA [8] is shown in Figure 2. Six variations of the standard barge were also designed to cover the range in variation of dimensions and physical characteristics for typical barges. A total of seven design “Cases” were set up as follows:

1. Long Barge
2. Short Barge
3. “Standard” (Parent) Barge ( $T_n = 10$  sec.)
4. Deep Draft Barge
5. Shallow Draft Barge
6. Short Roll Period Barge ( $T_n = 6$  sec.)
7. Long Roll Period Barge ( $T_n = 15$  sec.)

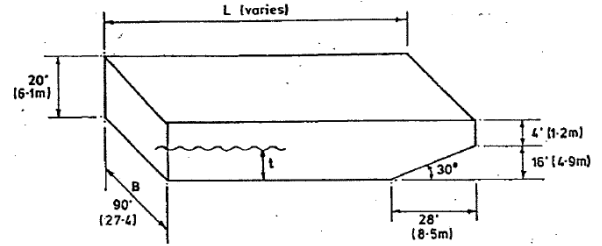


Figure 2 – Standard Barge Configuration

L = 300 ft. (91.242 m)

(Courtesy, Noble Denton & Associates)

## 2. BARGE ROLL MOTION ANALYSIS

To perform an equivalent linearization of the barge motions it was necessary to develop frequency domain software to compute the roll motions. This process is outlined below. To start with, the nonlinear time domain roll equation to be linearized is shown below.

### 2.1 Time domain equation of motion

The time-domain equation of barge roll motion with nonlinearities in roll damping is given as follows:

$$(I_{xx} + A_{44}) \frac{d^2(\phi)}{dt^2} + M_D + C_{44} \phi = F_4(t) \quad (1)$$

Where:

- $\phi$  = Roll angle
- $W$  =  $Mg$  = Weight displacement
- $I_{xx}$  = Vessel's roll moment of inertia
- $C_{44}$  =  $W \times GM_T$  = Hydrostatic restoring moment coefficient
- $A_{44}$  = Hydrodynamic moment of inertia in roll
- $M_D$  = Damping (velocity-dependent) moment
- $GM_T$  = Transverse metacentric height
- $F_4(t)$  = Roll excitation moment
- $M$  = Vessel's mass displacement
- $g$  = Gravitational acceleration

For larger amplitudes of motion, the roll damping moment  $M_D$  is highly nonlinear, frequently modeled using a Morison's-type  $v|v|$  term [9] associated with fluid dynamic pressure forces. The nonlinear roll damping moment including a cubic term can be written as follows:

$$M_D(t) = K_1 d\phi/dt + K_2 d\phi/dt |d\phi/dt| + K_3 (d\phi/dt)^3 \quad (2)$$

where  $K_1$ ,  $K_2$ , and  $K_3$  are the linear, Morison-type and cubic damping coefficients, respectively, and  $d\phi/dt$  is the angular velocity  $\omega$ .

### 3.2 Frequency domain equation of motion

The nonlinear time-domain equation of motion (Eqns 1 & 2) can be converted into a linear form using the above-mentioned equivalent linearization procedure [1], [2], and [4]. The

corresponding complex frequency-domain equation of motion is written as follows:

$$\{ [C_{44} - (I_{xx} + A_{44}) \omega^2] + i M_D(\omega) \} \phi(\omega) = F_4(\omega) \quad (3)$$

where,

$i$  = Imaginary unit,

$\omega$  = Cyclic frequency.

The roll angle  $\phi(\omega)$  and external moment  $F_4(\omega)$  are now frequency dependent complex numbers.

The damping moment term can be expressed in the frequency domain in this form:

$$M_D(\omega) = \omega b^L(\omega) \quad (4)$$

Where  $b^L(\omega)$  = Frequency-dependent damping coefficient.

The complex roll  $\phi(\omega)$  and moment  $F_4(\omega)$  may be broken down into real and imaginary components as follows:

$$\phi(\omega) = \phi_R(\omega) + i \phi_I(\omega) \quad (4a)$$

$$F_4(\omega) = F_{4R}(\omega) + i F_{4I}(\omega) \quad (4b)$$

The roll motion components can then be written from (Eq. 3) as follows:

$$\phi_R(\omega) = \frac{[F_{4R}(C_{44} - \omega^2 A_{44}) + \omega b^L(\omega) F_{4I}]}{[(C_{44} - \omega^2 A_{44})^2 + (\omega b^L)^2]} \quad (5a)$$

and,

$$\phi_I(\omega) = \frac{[F_{4I}(C_{44} - \omega^2 A_{44}) + \omega b^L(\omega) F_{4R}]}{[(C_{44} - \omega^2 A_{44})^2 + (\omega b^L)^2]} \quad (5b)$$

Finally, the roll phase angle can be written as:

$$\theta(\omega) = \text{atan}(\phi_I/\phi_R)$$

### 3.3 Calculation of roll motion frequency response functions

For use in comparison with the NDA model roll test data, the roll motion equations (5a) and (5b) were used to calculate the roll angles as a function of frequency for all seven barge cases. The calculations were performed on Excel spread sheets. The barge physical properties including non-dimensional hydrodynamic coefficients and roll moment  $F_4(\omega)$  coefficients were obtained from the NDA report and, where necessary, hand calculations were performed.

### 3.4 Response Amplitude Operators (RAOs)

The NDA roll motion magnitude data was presented in the NDA report in the form of response amplitude operators (RAOs) with dimensions of (deg/m) for all seven cases. In the present study RAOs were computed both as roll per unit wave height and as roll angle per unit wave slope. The per unit wave slope RAO was preferred for analysis purposes as it is a pure dimensionless number indicating the magnification of the wave excitation, and is more useful for interpretation.

### 3.5 Equivalent linear damping

The main purpose of the investigation was to model the nonlinear roll response using the equivalent linearization technique. The nonlinear behavior of interest here is the drastic roll peak falloff with roll amplitude as shown in Figure 1. This nonlinear behavior is characterized by variation of the roll damping with frequency. This frequency variation can be modeled using the equivalent linear damping function  $b^L(\omega)$ . This damping function is usually expressed as a three-term series expansion of parabolas as follows [1], [2], [5]:

$$b^L(\omega) = C_1 + 8/(3\pi) C_2 (\omega\phi_0) + 1/4 C_3 (\omega\phi_0)^2 \quad (6)$$

where  $C_1$ ,  $C_2$ , and  $C_3$  are the adjustable constant, linear and square-law coefficients, respectively, and  $\phi_0$  = Peak roll angle at the roll resonance frequency  $\omega_n$ .

Note that Eqn (6) is a truncated power series that can be generalized as:

$$b^L(\omega) = C_1 + \sum_2^{\infty} C_k \alpha^k (\omega\phi_0)^k, \quad (6-a)$$

where  $\alpha^k$  is a fixed constant factor.

Note also that  $(\omega\phi_0)$  in (6) and (6-a) is the expansion parameter. Note that the expansion factor evaluated at the natural frequency ( $\phi_0\omega_n$ ) is the maximum roll angular velocity of the vessel for a given wave height. To give specific values for these physical quantities, consider the Case 3 standard barge in a 3 meter high wave having a maximum roll angle of 26 degrees. The vessel's natural period of 10 seconds corresponds to a frequency  $\omega_n = 0.625$  rad/sec. For this case, the value of the expansion parameter ( $\omega_n\phi_0$ ) is 0.284 rad/sec, or 16.3 degrees per second.

It will be shown later that the generalized expansion (6-a), with more terms in the power series, should be able to provide more accurate curve-fitting to experimental data. For curve fitting, it is more convenient to use a frequency-shifted form of the expansion (6 or 6-a) that is centered at the natural frequency  $\omega_n$ , as shown below:

$$b^L(\omega - \omega_n) = C_1 + \sum_2^{\infty} C_k [(\omega - \omega_n)\phi_0]^k. \quad (6-b)$$

This form is more convenient because  $C_1$  is then the linear damping coefficient and the power series terms are corrections representing the nonlinear effects. The expansion (6-b) is a series of  $k^{\text{th}}$  order even or odd parabolas centered at the natural frequency. This form represents a mechanical filter useful for curve-fitting the computed RAOs.

#### 4. COMPARISON OF COMPUTED RAOS WITH TANK TEST DATA

Plots of RAOS and phase angles were prepared for each load case and wave height tested using the motions equations (5-a and 5-b), and the results were compared to the NDA data. Good agreement at the RAO roll peak was achieved by adjusting the (constant linear)  $C_1$  damping coefficient. The shape of the computed RAO peaks or “humps” were consistently narrower or steeper than the wave tank-produced RAO data. This can be seen in Figure 3, which is the Case 3 RAO for a 3 m wave. On the plot the wave tank data is shown as data points, while the computed data is the continuous line. This same narrow computed peak shape was evident for all seven cases. Fair agreement with the test data is seen, except that the computed resonance peak is too narrow. A remedy for this problem will be discussed later.

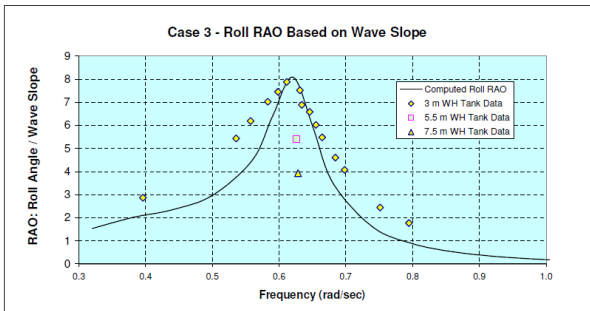


Figure 3 – Roll RAO for Case 3 (Standard Barge) in 3 m Beam Seas Regular Wave

A comparison plot of phase angle data for Case 3 is shown in Figure 3. Fair agreement is seen, except that the computed phase angle is indicating too much damping.

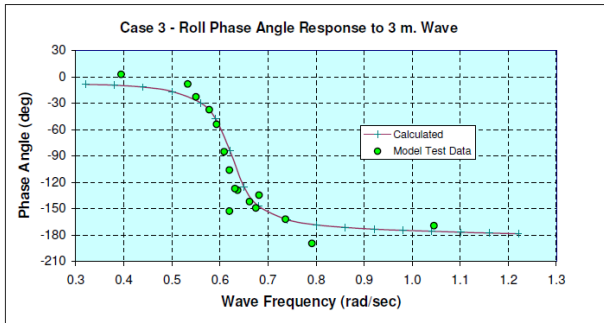


Figure 3 – Roll Phase Angle for Case 3 in a 3 m Wave

#### 4.1 Peak matching

The roll peak matching procedure is a multi-step (manual) curve-fitting process where the calculated data peak is matched to the experimental data peak. This is done by varying only the constant  $C_1$  term in the expression for  $b^L(\omega)$  in Eq. 6. ( $C_2$  and  $C_3$  are set to zero.) As mentioned before, the constant damping value  $C_1$  corresponds to the linear response. The curve fitting is done by trial and error varying  $C_1$  until the computed peak matches the experimental data. Increasing the

value of  $C_1$  causes peak to drop, while decreasing  $C_1$  causes the peak to rise up. The value of  $C_1$  where the peaks match can be denoted as  $b^L$ . Table 1 shows the results of the peak – matching process for all the barge cases and all the wave heights tested. Other test conditions are also presented.

Case no.	Wave Ht m	$\omega_n$ rad/sec	$T_n$ sec	RAO Peaks		Roll Peak deg	Wave Slope deg	b44v MN/s
				deg/m	deg/deg			
1	3.0	0.640	9.82	6.60	5.50	19.8	3.590	1.80E+05
2	3.0	0.650	9.67	7.90	6.45	23.7	3.703	7.70E+04
2	6.0	0.640	9.82	5.30	4.50	31.8	7.180	3.50E+05
3	3.0	0.620	10.13	8.70	8.00	26.1	3.369	1.43E+05
3	5.5	0.620	10.13	6.20	5.40	34.1	6.177	4.30E+05
3	7.5	0.620	10.13	4.50	4.90	33.75	8.423	8.35E+05
4	1.5	0.665	9.45	10.40	9.20	15.6	1.938	4.80E+04
4	3.0	0.660	9.52	4.40	4.50	13.2	3.818	2.80E+05
4	7.0	0.588	10.69	3.00	2.50	21.0	7.071	1.52E+06
5	1.5	0.610	10.30	10.00	9.20	14.0	1.631	3.75E+04
5	3.0	0.615	10.22	7.30	6.80	20.4	3.315	1.77E+05
5	5.5	0.610	10.30	5.50	5.00	27.5	5.979	5.30E+05
6	1.5	1.035	6.07	8.80	2.80	13.2	4.694	6.00E+04
6	3.0	?	?	?	?	?	?	1.00E+05
7	1.5	0.440	14.28	10.25	18.40	15.375	0.848	6.00E+04
7	3.0	0.440	14.28	7.80	14.00	23.4	1.697	1.70E+05
7	6.0	0.440	14.28	4.78	8.45	28.68	3.394	5.75E+05
7	7.6	0.440	14.28	4.20	6.60	31.92	4.299	1.00E+06

Table 1 – Summary Table of Test Conditions and Linear Damping Coefficients For All Seven Barge Cases

#### 4.2 Two-term equivalent linearization procedure

The frequency domain equivalent linearization representation of the roll damping (Eqn.6) may be used to shape the damping curves so that the responses better match the experimental roll data. This curve-fitting of the RAOs is done by adjusting the  $C_1$ ,  $C_2$ , and  $C_3$  coefficients until the roll angle curves agree as well as possible. This matching can readily be done for two-term fits on a trial and error basis, as described below.

#### 4.3 Step by step two term trial and error peak matching

1. Start by selecting any value for the slope constant  $C_2$ .
2. Select a value  $C_1$ .
3. Vary  $C_1$  until the computed peak matches up with the measured peak.
4. Select another value for  $C_2$ .
5. Repeat the procedure.

One will discover that good matching can be achieved for any  $C_2$  by selecting a proper value for  $C_1$ . Several fits were made this way, and the values of  $C_1$  and total damping coefficient  $b^L(\omega)$  were plotted against the slope constant  $C_2$ . The results show a straight-line relation for  $C_1$  and  $b^L(\omega_n)$  as a function of  $C_2$ . These results indicate that there is no unique (or even preferred) solution for the two-term peak matching procedure. This is because varying  $C_2$  did not noticeably affect the shape of the response curve. This was surprising, as one would expect the frequency variation to significantly affect the RAO shape.

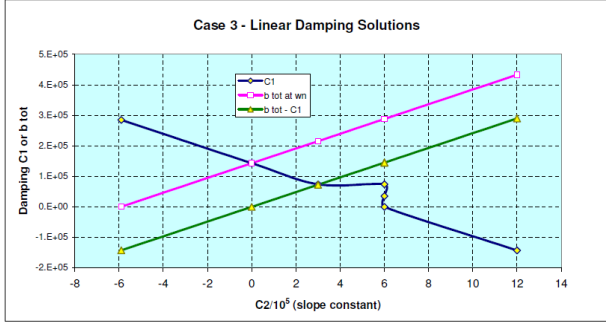


Figure 4 – Linear (2-Term) Damping Curve-Fit Results

#### 4.4 Frequency shift for two-term fit

One can obtain valuable insight into the two-term damping procedure by doing a frequency shift by referencing the frequency dependence relative to the natural frequency  $\omega_n$ . This is done by taking the shifted two-term formulation from Eqn 6-b, and reformulating the expression with the modified constant term. The result is as follows:

$$b^L(\omega_n) = (C_1)^N + 8/(3\pi) C_2 \phi_0(\omega - \omega_n) \quad (7)$$

where  $(C_1)^N = C_1 + 8/(3\pi)C_2(\omega_n\phi_0)$

In Eqn. (7), The term  $(C_1)^N$  is the new constant “ $C_1$ ”, or y-intercept, and the second term is a straight line with its origin at  $\omega = \omega_n$ , with a slope  $8/(3\pi) C_2$ . One sees that the damping curve acts like an asymmetric damping filter, amplifying the damping to the right of  $\omega_n$  and attenuating it to the left. This means the roll response will be reduced to the right and increased to the left. This effect of the filter was not large enough to be detected on the RAO plots for the range of slope  $C_2$  seen in Figure 4. Note that if the slope is too steep the damping will be negative when the damping line crosses the  $b = 0$  line. This is physically impermissible.

#### 4.5 Connection between RAO curve shape and spectral response

Figure 3 shows how the computed RAO has, in the vicinity of the natural frequency, a peak or “hump” shape that is too narrow compared to the wave tank data. This is a problem if one wants to do random wave spectral response calculations. This is because the square of the area under the RAO magnitude curve is used in the spectral calculations. The responses will be under-predicted using the computed RAO data because the slim “hump” area will be less than the model test RAO’s area. This under prediction of motions was observed in the NDA study [7]. The effect of the area under the RAO can be seen from the spectral response equation for roll angle:

$$\sigma_{\phi}^2 = \int_0^{\infty} S(\omega) |H_{\phi}(\omega)|^2 d\omega, \quad (8)$$

where  $\sigma_{\phi}^2$  is the variance of the roll angle,  $S(\omega)$  is the unidirectional wave spectrum, and  $|H_{\phi}(\omega)|$  is the amplitude of the roll angle.

#### 4.6 Designing a parabolic damping filter to improve RAO shape and correlation with test data

It is possible to broaden the computed RAO “hump” to better fit the wave tank data by using a properly designed mechanical/fluid mechanics filter. The narrow RAO hump can be broadened by raising up the local RAO amplitude values in the frequency ranges away from the natural frequency ( $\omega_n$ ) peak. Raising up the RAO requires a reduction of the damping locally. This damping reduction can be achieved by introducing a parabolic filter with a shape as shown in Figure 5. At the natural frequency of 0.625 rad/sec the filter damping has the value obtained by the peak matching procedure discussed earlier. Figure 5 shows the parabolic filter shape used at the optimum  $C_3$  value of  $1.5 \times 10^6$ .

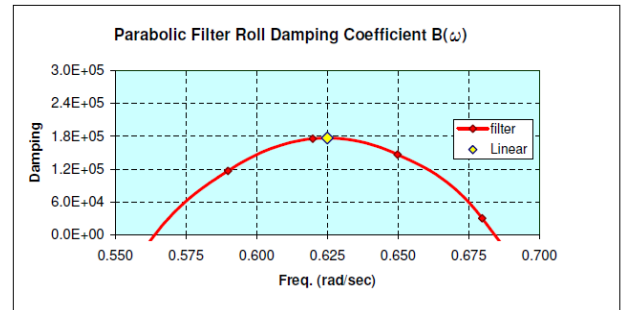


Figure 5 – Roll Damping Coefficient as a Function of Frequency for Parabolic Filter

The parabolic filter equation used has the following form:

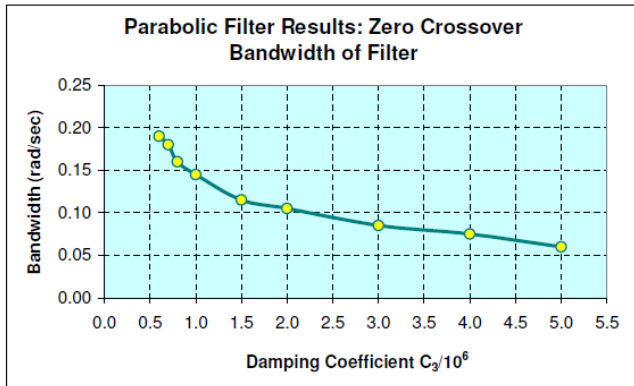
$$b_F(\omega) = -32.65 K_F (\omega - \omega_n)^2, \quad (9)$$

where  $b_F(\omega)$  = Filter damping coefficient,  
and  $K_F$  =  $C_3$  = Magnification factor.

The constant (32.65) was calculated to provide a steep curve with the proper bandwidth at  $K_F = 1.0$ . Equation (9) was not developed by using an equivalent linearization form. There were difficulties in constructing a properly shaped curve using the equivalent linearization expansion. To properly construct a suitable filter shape using equivalent linearization, higher order terms must be used. This form (Eqn. 9) was used solely to demonstrate the concept of using a (mathematical) damping filter form to provide a better fit to the wave tank RAOs over a limited frequency range. From Fig. (5) one can define the filter bandwidth as the frequency distance between the zero-crossings. Outside this bandwidth the damping is negative, indicating that energy is being fed into the vessel, which is physically unrealistic. This means that the filtered RAO values are only valid inside the bandwidth.

#### 4.7 Results of using the parabolic damping filter to improve RAO shape and correlation with test data

The Case 3 RAOs with the filter were calculated for a range of filter magnification values  $C_3$ . The bandwidths and other data were recorded for each value of  $C_3$ . The bandwidth results are shown in Figure 6. One sees that the bandwidth decreases with increasing  $C_3$ . This means that the range of valid (non-negative damping) data decreases with increasing  $C_3$ .



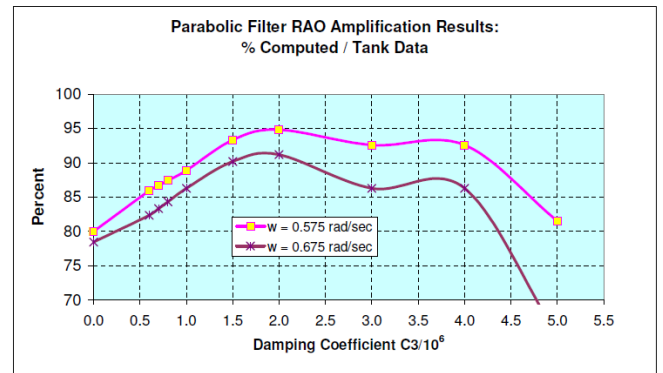
**Figure 6 – Parabolic Filter Results: Zero Crossover Bandwidth as a Function of  $C_3$**

Figure 7 was prepared to illustrate how the parabolic filter provides amplification to the computed response, improving correlation with the tank test data. Responses at two frequencies are shown: one at  $\omega = 0.575$  rad/sec, and the other at  $\omega = 0.675$  rad/sec. The first is slightly below the natural frequency ( $\omega_n$ ) of  $0.625$  rad/sec, and the other is slightly above. One sees from Figure 7 that the maximum amplification occurred at  $C_3 = 2.0 \times 10^6$ . At that point, the computed, filtered response was 95% of the wave tank result at  $\omega = 0.575$  rad/sec, and 92% at  $\omega = 0.675$  rad/sec. At  $C_3 = 0$  (no filter) the respective percentages were 80% and 78%, indicating that the presence of the filter provided a considerable improvement in accuracy. These results are shown in Table 2 below:

**Table 2 – Percent Agreement with Test Data Due to Filter**

Frequency (rad/sec)	Percent with filter	No Filter	% Difference
0.575	95	80	15
0.675	92	78	14

Beyond the  $C_3 = 2.0 \times 10^6$  point, the responses deteriorate because of the narrowness of the bandwidth.



**Figure 7 – Local RAO Amplification Due to Filter as a Function of the  $C_3$  Filter Damping Coefficient**

Table 3 was prepared to present additional data on the effects of the filter for ten values of the filter amplification constant  $C_3$ . The first two columns show the values of the filter constant used. The RAO readings for the first frequency (0.575) are given in the next two columns. The RAO readings for the higher frequency (0.675) are given in the following two columns. In the next two columns the filter frequency zero crossings are given: first for the lower frequency, and the next for the higher frequency. In the following column the filter bandwidth, computed by taking the difference between the higher cutoff frequency and the lower are shown. Finally, comments on the response are given in the last column. The data shows that the optimum  $C_3$  value was  $1.5 \times 10^6$ . (See also Figure 7.) This value gave the highest level of amplification before the response starts to deteriorate due to the narrowing of the filter bandwidth. At the narrower bandwidths, the damping becomes negative over a wider frequency range. The extensive negative damping deteriorates the RAO shape. It first becomes lopsided at  $C_3 = 2 \times 10^6$ . After this it develops a double-humped peak that gets worse as  $C_3$  increases. (See comments on last column.)

**Table 3 – Parabolic Filter Data as a Function of  $C_3$ , the Filter Amplification Constant**

Damping Coefficient		Tank Ht 6.75 RAO Ht, $\omega =$ 0.575	Percent Wave Tank Value	Tank Ht 5.1 RAO Ht $\omega = 0.675$	Percent Wave Tank Value	Filter Zero Crossing Frequencies (rad/sec)		Filter Band Width (rad/sec)	Comments
$C_3$	$C_3/10^6$					Lower	Higher		
0	0.0	5.400	80.00	4.000	78.43	n/a	n/a	n/a	No Filter
6.00E+05	0.6	5.800	85.93	4.200	82.35	0.530	0.720	0.190	normal RAO
7.00E+05	0.7	5.850	86.67	4.250	83.33	0.535	0.715	0.180	normal RAO
8.00E+05	0.8	5.900	87.41	4.300	84.31	0.545	0.705	0.160	normal RAO
1.00E+06	1.0	6.000	88.89	4.400	86.27	0.550	0.695	0.145	normal RAO
1.50E+06	1.5	6.300	93.33	4.600	90.20	0.565	0.680	0.115	Optimum RAO
2.00E+06	2.0	6.400	94.81	4.650	91.18	0.570	0.675	0.105	lop sided RAO
3.00E+06	3.0	6.250	92.59	4.400	86.27	0.580	0.665	0.085	dbl peak RAO
4.00E+06	4.0	6.250	92.59	4.400	86.27	0.585	0.660	0.075	dbl peak RAO
5.00E+06	5.0	5.500	81.48	3.300	64.71	0.595	0.655	0.060	dbl peak RAO

**4.6 Improvement in RAO shape due to filter**

Figure 8 shows the RAO correlation with the filter, and Figure 9 shows it without the filter. 1. The comparison shows that the shape of filtered RAO was greatly improved, at least over the limited frequency range for which the filter was designed. The improvement in the computed RAO response due to the filter is clearly seen by comparing Figures 8 and 9, both plotted over a narrower frequency range than in Figure 33..

**4.7 Comments on damping filter results**

It should be clear that the computed filtered response in Figure 8 has the more realistic wider peak agreeing better with the test data points than the unfiltered results in Figure 9. This indicates that it should be feasible to filter the computed responses to agree well with tank test data over the full frequency range using an extended power series equivalent linearization procedure, once such a procedure is available.

**5. CONCLUDING COMMENTS**

1. The roll angle peak nonlinearity in the time domain manifests itself physically in the frequency domain as a frequency-dependent roll damping function.
2. Because of this, the extreme roll angle nonlinearity is most conveniently analyzed in the frequency domain.
3. The time-domain equation of motion in roll has a number of nonlinear damping terms. Therefore, to analyze the problem in the frequency domain, an equivalent linearization procedure must be applied to the damping terms.
4. The “equal energy” equivalent linearization procedure appears to be most convenient to use because of its simplicity. This procedure involves equating the damping energy for each nonlinear damping term in one cycle of oscillation, to the energy in the corresponding equivalent linear term.
5. To evaluate each damping constant, a curve-fitting procedure for the RAO must be performed. For each term the constant is adjusted so that the computed RAO conforms to the experimentally-obtained RAO.
6. To use the RAOs obtained from the equivalent linearization for spectral (random wave) calculations, their areas must be the same, or very close to, those of the test data.
7. The current equivalent linearization procedure for the damping coefficient expansion has only three terms.
8. The 3-term expansion proved inadequate to filter the damping so that a good fit could be made.
9. Therefore, a parabolic filter was used to obtain improved correlation of the RAO with the test data over a limited frequency range.
10. The filter improved correlation with the wave tank data, demonstrating the feasibility of using an equivalent linear expansion to accurately model the test data. .

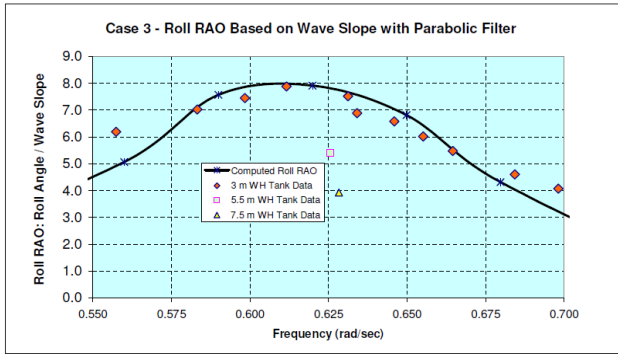


**Figure 8- Comparison of Computed RAO Using Optimum Parabolic Filter vs. Test Tank Data**

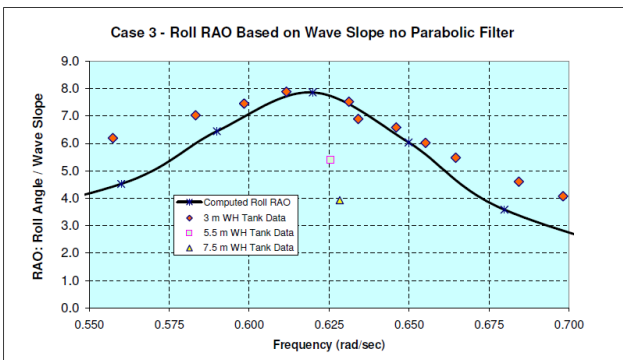


**Figure 9 – Comparison of Computed Roll RAO with no Filter vs. Test Tank Data**

11. To improve the RAO fit over the full frequency range, higher-order terms in the equivalent linearization expansion will have to be calculated.

12. A more complex filter shape has to be designed and implemented to achieve good correlation. A bell-shaped filter, requiring an expansion to perhaps the sixth or eighth order should provide enough resolution to use the RAO in random wave spectral work.

13. Such a filter will eliminate negative damping.

14 Implementing this would require a more sophisticated curve-fitting procedure, possibly based on a least-squares scheme.

15. Analysis of the shape of the frequency domain roll damping function should provide useful insight into the fluid dynamics of the nonlinear roll damping mechanisms. This will most likely involve nonlinear ship-wave interaction.

16. In conclusion, this procedure has great promise for generating realistic RAOs for use in spectral work, and as a hydrodynamics research tool. As such, the implementation of the procedure should contribute significantly to the state of the art in the field of nonlinear ship roll motions.

## 6. RECOMMENDATIONS

To increase the value and effectiveness of the equal energy equivalent linearization procedure, the following tasks are recommended:

1. To improve the accuracy of the RAO curve-fitting procedure, extend the equivalent linearization expansion from the third to the 6<sup>th</sup> or 8<sup>th</sup> order.
2. To facilitate the curve fitting process, develop a least-squares or similar curve fitting procedure for use with the higher order expansion.

Taking these steps should improve the shape of the calculated RAO so that it agrees well with wave tank data. This would make it feasible to use calculated RAOs in random wave spectral response calculations, thus greatly increasing the usefulness of the equivalent linearization procedure. In addition, information on the frequency domain roll damping can be used as a hydrodynamics research tool in the investigation of nonlinear ship-wave interactions.

## 8. REFERENCES

[1] Ibrahim, R. A., Grace, I. M., "Modeling of Ship Roll Dynamics and Its Coupling with Heave and Pitch.", *Mathematical Problems in Engineering*, Vol. 2010, Article ID 934713, 2010.

[2] A. F. El-Bassiouny, "Nonlinear Analysis for a Ship with a General Roll-Damping Model, *Physica Scripta*, vol. 75, no. 5, pp. 691–701, 2007.

[3] Dhavalikar and Negi, "Estimation of Roll Damping for Transportation Barges", *Proc.Of ASME International Conference on Ocean, Offshore and Arctic Engineering*, 2009.

[4] Faltensen, Odd M. "Sea Loads on Ships and Offshore Structures", *Cambridge Ocean Technology Series*, 1990.

[5] Magnuson, Allen H., "A Reanalysis of Barge Roll Motion Data", *Slideshow Presentation, Society of Naval Architects and Marine Engineers, Houston, Texas Section Meeting*, January, 2007.

[6] S. Ando, "On the Improvement for Various Performances of Work Vessels", *Transactions of the West Japan Society of Naval Architects*, No. 50, August, 1975, pp. 83-98.

[7] Robert Latorre, "Improvement of Barge Towing: Translations of Selected Japanese and Russian Technical Articles", *Report No. 226, The Department of Naval Architecture and Marine Engineering, The University of Michigan, College of Engineering*, May 1980.

[8] (Anon.) Noble Denton & Associates Ltd., "Barge Motion Research Project: Summary Report", *Report No. L12140/NDA/JBW*, July 1984.

[9] J. P. Morison, M. P. O'Brien, J. W. Johnson, and S. A. Schaaf, "The force exerted by surface waves on a pile," *Petroleum Transactions*, vol. 189, pp. 149–154, 1950.